A Computational Study of the Adsorption of Small Ag and Au Nanoclusters on Graphite†

Jukka-Pekka Jalkanen,‡,§ Marjo Halonen,‡,|| Delia Fernández-Torre,‡ Kari Laasonen,# and Lauri Halonen*,‡

Laboratory of Physical Chemistry, P.O. Box 55 (A.I. Virtasen aukio 1), FIN-00014 University of Helsinki, Finland, and Department of Chemistry, P.O. Box 3000, FIN-90014 University of Oulu, Finland

Received: June 26, 2007; In Final Form: September 3, 2007

The adsorption of silver and gold atoms, and M_2, M_6, and M_{13} (M = Ag or Au) clusters on the (0001) graphite surface has been investigated computationally using the density functional theory (DFT) with periodic boundary conditions and plane wave basis functions. The surface has been modeled as a single carbon sheet. The role of dispersion forces has been studied with an empirical classical model. The results show that the clusters avoid hollow sites on the graphite surface, and that the metal atoms favor atop and bond sites. Large structural changes are observed in octahedral M_6 and icosahedral M_{13} clusters on the graphite surface when compared with gas-phase geometries. The results also indicate that if accurate results are required, the dispersion forces between metal and carbon atoms should be included in the studied systems.

1. Introduction

An understanding of the energetics of isolated metal clusters adsorbed on different sites of semiconductor surfaces is required to model both the interaction between the clusters and the formation of large structures such as nanowires on these surfaces. Modern electronic structure calculation theories such as Møller−Plesset perturbation theory (MP) and density functional theory (DFT) allow the quantitative study of small clusters on surfaces. The starting point for this work is a calculation of the properties of isolated clusters and a comparison with experimental data, such as adsorption energies and structures when available. The structural changes of the clusters close to surfaces, when compared with gas-phase values, are also interesting, because there is currently little quantitative experimental information on this. These structural changes are often so large that the usual definition of adsorption energy does not give the best physical measure of the quantity. In the extreme case, the clusters break into free atoms, i.e., the atoms wet the surface.

The nature of the interaction between the surface and the cluster is interesting. The interaction between the cluster and the mirror induced dipole inside the surface is a possibility, but one should not ignore the role of van der Waals (dispersion) forces, which can be significant even in describing plain surfaces such as graphite. The modeling of dispersion forces, which arise from electron correlated effects, is demanding in the density functional theory because their effects are excluded from standard functionals. These forces are included in some other electronic structure calculation theories such as the MP, but unfortunately these present some other problems such as often being limited to atomic basis sets and being computationally expensive.

In this work, we study the structure and binding energies of small nanoclusters of Ag and Au adsorbed on the nondefective (0001) surface of graphite. We use the DFT method with periodic boundary conditions and plane wave basis sets. Owing to the limited computational resources at our disposal, we discuss only atoms and the small clusters M_2, M_6, and M_{13}, where M = Au or Ag. We have chosen this set because atoms and dimers are natural test cases for computational methods, and isolated M_6 and M_{13} clusters form symmetrical three-dimensional structures (octahedral and icosahedral, respectively), whose deformation on surfaces is worth studying. We first treat each of these as an isolated system, and then as adsorbed species on graphite, which has been modeled as a single carbon sheet. All of the gas-phase clusters have been investigated computationally in detail previously,[1−5] so we describe only briefly our results for these systems. The adsorption of atoms and dimers of Ag and Au on graphite has also been studied previously with the DFT method, although mainly with a local density approximation (LDA).[6−10] In our contribution, we model these systems by employing the generalized gradient approximation (GGA), which often produces different results from the LDA approach. Finally, there is also a previous DFT study of a planar Au_6 cluster adsorbed on graphite.[11] To our knowledge, the adsorption on graphite of Ag_6, three-dimensional Au_6 clusters, and the M_{13} structures has not been studied by DFT methods previously.

We also present an estimation of the long-range dispersion binding energies in the systems studied. As far as we know, dispersion effects on metallic clusters adsorbed on the graphite surface have not previously been studied computationally. Because the current standard functionals in the DFT theory exclude long-range electron correlations,[12−16] we have adopted semiempirical approaches that can be employed on top of the DFT energies to account for dispersion.[17,18] This strategy has been successful in some systems of biological interest[17] because, once properly refined, these models capture the behavior of dispersion forces well, and they are conceptually simple, and computationally cheap.

† Part of the "Giacinto Scoles Festschrift".

* To whom correspondence should be addressed. E-mail: lauri.halonen@helsinki.fi.

‡ University of Helsinki.

§ Present Address: Finnish Meteorological Institute, PO Box 503, FIN-00101 Helsinki, Finland.

University of Oulu.

|| Present address: Department of Food Technology, P.O. Box 66, FIN-00014 University of Helsinki, Finland.

10.1021/jp074969m CCC: $37.00
Published on Web 11/01/2007

2. Method

2a. Electronic Structure Calculations. All electronic structure calculations were performed using the Vienna *ab Initio* Simulation Package (VASP), a plane wave based density functional theory code capable of describing periodic systems. The projector augmented wave (PAW) method[19,20] and generalized gradient approximation (GGA) Perdew−Wang 91 exchange correlation functional[21] as implemented in VASP were chosen for their good performance in describing the energetics of small metal clusters. Test calculations with norm-conserving ultrasoft pseudopotentials and the local density approximation (LDA) were also conducted on a silver atom on graphite, but these computations overestimated binding energies when compared with the GGA results. For comparison, PAW/PBE (Perdew−Burke−Ernzerhof) potentials were also used in the case of an Ag or Au atom adsorbed on graphite but these gave similar results to the PAW/PW91 potentials.

The graphite surface was modeled with a single layer of 96 carbon atoms, but test calculations with two, three, and four layers of graphite were performed and deemed unnecessary due to the small effect of the additional layers on cluster adsorption energetics and structure. The large dimensions of the fully relaxed surface slab (14.8 Å × 17 Å) were necessary to avoid interactions between adjacent metal clusters (1 Å = 10^{-10} m). This was especially challenging for the largest (M_{13}) clusters included in this work. Taking into account the size of the largest clusters and computational limitations, a vacuum region of 25 Å was used to separate the slabs from each other.

The irreducible number of **k**-points was used as a parameter to check the **k**-point mesh convergence. In our case, the **k**-point sets $n \times n \times 1$, where $n = 2-5$, correspond to the irreducible number of **k**-points 4, 5, 10, and 13, respectively. Generally, a Γ-centered mesh of $2 \times 2 \times 1$ **k**-points and a cutoff energy of 400 eV were found to be adequate, but in the case of atoms adsorbed on graphite a **k**-point mesh $3 \times 3 \times 1$ and a cutoff energy of 500 eV were needed (1 eV = 0.160 218 aJ). Convergence tests were also made with the **k**-point sets $4 \times 4 \times 1$ and $5 \times 5 \times 1$ in the case of the dimer adsorbed perpendicularly above the atop site of the graphite surface. The effect of inclusion of spin polarization was tested and deemed negligible except for single metal atom, isolated non-planar M_6, and isolated M_{13} energies, where spin polarized calculations were performed.[22] All forces were optimized until the values were less than 30 meV/Å.

As opposed to semirigid molecular systems, the structure of large metal clusters may change greatly near a surface, and there can be substantial energy changes due to the rearrangements of atoms. Therefore, there is no unique way to define the adsorption energy. We have used the following three definitions

$$E_1 = E(\text{system}) - E(\text{surface, vacuum}) - E(\text{cluster, vacuum}) \quad (1)$$

$$E_2 = E(\text{system}) - E(\text{surface, vacuum}) - n \times E(\text{metal atom, vacuum}) \quad (2)$$

$$E_3 = E(\text{system}) - E(\text{surface, adsorption}) - E(\text{cluster, adsorption}) \quad (3)$$

In the first definition, we subtract from the system energy the energies of the individual components obtained after a vacuum optimization. However, when significant structural distortion occurs, the energies obtained in this way contain deformation energy as well as the interaction energy between the surface and the adsorbed cluster. The second definition removes this factor, but it contains the interaction energy between the surface and the cluster plus the cohesive energy that is gained when atoms are organized into a cluster. The third definition subtracts the energy of adsorption structures from the total system energy and represents only the interaction energy between the surface and the cluster once they have been reorganized to form the adsorption system.

2b. Estimation of van der Waals Dispersion Energies. We mainly follow the methodology proposed by Elstner[17] to estimate dispersion energies. We also apply Grimme's approach[18] to the silver−graphite system to compare the results from the two different approaches.

The dispersion energy is modeled by means of an R^{-6} term in Elstner's proposal as follows

$$E_{\text{VdW}} = -\sum_{\substack{i,j \\ j>i}} f(R_{ij}^{(\alpha\beta)}) \frac{C_6^{(\alpha\beta)}}{(R_{ij}^{(\alpha\beta)})^6} \quad (4)$$

where $R_{ij}^{(\alpha\beta)}$ stands for the distance between atoms i and j, whose atomic species are α and β, $C_6^{(\alpha\beta)}$ is a coefficient related to the strength of the van der Waals interaction between atomic species α and β, and $f(R_{ij}^{(\alpha\beta)})$ is a damping function that is used to provide a vanishing van der Waals interaction at short distances. Thus, with eq 4, a new term is added to the total DFT energy so that only the long distance behavior of the functional is modified. Different multiplicative scaling factors, which depend on the DFT functionals used, are often added to eq 4.[23] These can be found, for instance, by adjusting the DFT results to some high-level *ab initio* computations that accurately account for dispersion.

Elstner has adopted a method from Halgren[24] to estimate the C_6 coefficients. These can be calculated for the interaction of the same atomic type, αα, as

$$C_6^{(\alpha)} = \frac{3}{4}\sqrt{N_\alpha {p_\alpha}^3} \quad (5)$$

where N_α is the Slater−Kirkwood[25] number of electrons for the species α and p_α is the atomic polarizability. Equation 5 is written in atomic units and therefore the polarizability is expressed in bohr^3 to obtain the coefficient in hartree bohr^6. The C_6 coefficient for different atomic species, α and β, can be obtained from the C_6 coefficients of the identical atoms, αα, and $\beta\beta$, and the atomic polarizabilities, employing an empirical mixture rule as

$$C_6^{(\alpha\beta)} = \frac{2C_6^{(\alpha)}C_6^{(\beta)}p_\alpha p_\beta}{{p_\alpha}^2 C_6^{(\beta)} + {p_\beta}^2 C_6^{(\alpha)}} \quad (6)$$

Equation 6 appears in Elstner's paper with the indices in the denominator interchanged, which is probably a typographical mistake.

Halgren has observed empirically that the Slater−Kirkwood number of electrons grows linearly with the number of valence electrons of the atom. The range of atoms studied contains only the 14th to 18th column atoms and goes down to the Xe atom in the periodic table. Therefore, there is an empirical expression for the C atom, but not for Ag and Au, for which we use the equation proposed for atoms ranging from Sn to Xe. We have also searched for articles that propose values for the $C_6^{(\alpha)}$ coefficient of silver and have performed the calculations

employing the corresponding values.[26,27] We use the following extrapolation

$$\text{C}-\text{Ne}: \quad N_\alpha = 1.17 + 0.33N_V$$
$$\text{Sn}-\text{Xe}: \quad N_\alpha = 4.85 + 0.30N_V \tag{7}$$

where N_V is the number of valence electrons of the atom in question. The damping function $f(R_{ij}^{(\alpha\beta)})$ in eq 4 takes the form

$$f(R_{ij}^{(\alpha\beta)}) = [1 - e^{-d(R_{ij}^{(\alpha\beta)}/R_0^{(\alpha\beta)})^7}]^4 \tag{8}$$

where $d = 3.0$ in Halgren's method, and $R_0^{(\alpha\beta)}$ can be calculated from the van der Waals atomic radii as follows:[23]

$$R_0^{(\alpha\beta)} = \frac{(2R_{VdW}^{(\alpha)})^3 + (2R_{VdW}^{(\beta)})^3}{(2R_{VdW}^{(\alpha)})^2 + (2R_{VdW}^{(\beta)})^2} \tag{9}$$

We have also applied Grimme's method to silver clusters on graphite. This approach also employs eq 4. The $C_6^{(\alpha\beta)}$ coefficients are obtained in this approach as

$$C_6^{(\alpha\beta)} = \sqrt{C_6^{(\alpha)} C_6^{(\beta)}} \tag{10}$$

and the damping function as

$$f(R_{ij}^{(\alpha\beta)}) = \frac{1}{1 + e^{-d(R_{ij}^{(\alpha\beta)}/R_0^{(\alpha\beta)} - 1)}} \tag{11}$$

where $R_0^{(\alpha\beta)}$ is the sum of the atomic van der Waals radii and $d = 20$.

3. Results and Discussion: Graphite and Small Metal Clusters in a Vacuum

3a. Graphite. The description of graphite within the DFT is a difficult problem. The main component of the forces between the basal planes of graphite arises from weak van der Waals forces, which are not modeled well by the usual DFT codes. As a result, LDA functionals underestimate the interlayer binding energy of graphite but still predict a reasonable value for the interlayer distance.[28] Besides, GGA functionals fail to reproduce both the interlayer binding energy and the interlayer distance.[28]

We have also found that the DFT performs poorly with graphite; in particular, GGA functionals are unable to model the structure of graphite accurately and do not show significant binding between the layers. For this reason, the graphite surface is modeled as a single layer of carbon atoms. This approach decreases the number of different adsorption sites to three (atop, hollow, bridge) instead of separating the atop site into α and β sites as they would appear in a multilayer model of graphite. The surface was fully relaxed in all calculations allowing the deformation of the carbon atoms during cluster adsorption.

3b. Isolated Dimers. The structures of all metal clusters have been fully optimized and the calculated energies are collected in Table 1. The calculated equilibrium bond lengths of the dimers are in good agreement with the experimental values $r(Ag_2) = 2.53$ Å and $r(Au_2) = 2.47$ Å, being only a few hundredths of an Ångström larger. The tendency to slightly overestimate bond lengths is typical of GGA functionals. The cohesion energies from Table 1 also compare well with the experimental values, $E(Ag_2) = 1.65^1-1.67^{29}$ eV, and $E(Au_2) = 2.29^1-2.31^{29}$ eV. Binding energies are overestimated by about 0.5 eV with the LDA although both the LDA and GGA methods produce similar equilibrium bond lengths for silver and gold dimers.

TABLE 1: Calculated Energies and Nearest-Neighbor Distances of Small Metal Clusters

system	E (eV)[a]	d (Å)[b]
Au_2	−2.32	2.51
Au_6 octa[e]	−9.57	2.79
Au_6 planar	−11.58	2.79,[c] 2.64[d]
Au_{13} ico[e]	−24.97	2.93
Ag_2	−1.80	2.57
Ag_6 octa[e]	−7.55	2.80
Ag_6 planar	−8.76	2.79,[c] 2.69[d]
Ag_{13} ico[e]	−20.70	2.93

[a] Cohesion energies, $E = E(\text{cluster}) - nE(\text{atom})$, and n is the number of atoms. Ground state energies of Au and Ag atoms with spin polarization included are −0.152 and −0.172 eV, respectively. [b] Nearest-neighbor distances. [c] Nearest-neighbor distance in the interior triangle; see Figure 4. [d] Nearest-neighbor distance in the exterior triangle; see Figure 4. [e] Spin polarization included.

Because single Ag and Au atoms possess an electronic configuration $d^{10}s^1$, spin polarized calculations were performed for the atoms to obtain their ground state energies, which were used in calculating the bonding energy of clusters. Spin polarization has a negligible effect on dimers, and it was not applied. For example, an Au_2 dimer calculation yielded a total cluster energy of −2.624 eV neglecting the effect of spin polarization. A corresponding spin polarized calculation produced energies that are only 6 meV more negative.

3c. M_6 Structures. Octahedral and planar M_6 clusters have been investigated. Previous DFT studies on Ag_6[4] and Au_6[3] clusters suggest that the planar triangular clusters we consider (see Figure 4) are the lowest energy structures. The octahedral structure is energetically less favored, but it is an interesting model of three-dimensional clusters. The results presented in this article agree well with those of previous studies. Table 1 shows cohesive energies of planar triangular clusters to be about 0.34 (Au) and 0.22 eV/atom (Ag) more stable than the corresponding octahedral structures. The relaxed planar clusters possess an inner bond longer than the exterior bond. Structurally perfect octahedrons are obtained after relaxation.

3d. M_{13} Structures. Icosahedral clusters of Ag_{13} and Au_{13} have been fully optimized with spin polarization included and the results are presented in Table 1. The binding energy of a single gold atom differs little between icosahedral Au_{13} and planar triangular Au_6. However, the Ag_{13} icosahedron possesses about 0.1 eV/atom stronger binding energy than the planar Ag_6 cluster. Other M_{13} structures, including planar forms of Ag_{13} and Au_{13}, were not considered in this research, because adsorption studies would have required a considerable increase in surface slab dimensions, which would have been impossible due to computing limitations. Although it has been found that icosahedral structures are not the lowest in energy,[5] they provide a representative case from which to investigate structural changes in the neighborhood of semiconductor surfaces.

4. Results and Discussion: Adsorption Studies

4a. Single Atoms on Graphite. Both gold and silver clusters have been subject to intensive experimental and theoretical research.[6−11,30] The adsorption of single atoms has previously been studied with DFT methods, but most of those calculations were performed using the local density approximation (LDA), which often overestimates the binding as compared to the generalized gradient approximation (GGA). The published results are somewhat contradictory. On one hand, it has been

TABLE 2: Adsorption of Single Gold and Silver Atoms on Graphite[a]

atom/site	E_{ads} (eV)	$r_\perp$ (Å)	ΔZ_C (Å)[b]	E_{ads} (eV)/LDA	$r_\perp$ (Å)/LDA
Au, atop, 2 × 2 × 1, 400 eV[c]	−0.15	2.67	0.13		
Au, atop	−0.22	3.15	0.04	−0.67[d]	2.47[d]
Au, bond, 2 × 2 × 1, 400 eV	−0.16	3.17	0.02		
Au, bond	−0.22	3.21	0.03	−0.65[d]	2.48[d]
Au, hollow, 2 × 2 × 1, 400 eV	−0.16	3.43	−0.05		
Au, hollow	−0.22	3.41	0.04	−0.51[d]	2.62[d]
Ag, atop, 2 × 2 × 1, 400 eV[e]	0.09	2.69	0.07	−0.48	2.37
Ag, atop	−0.05	3.29	0.05	−0.44[f]	2.54[f]
Ag, bond, 2 × 2 × 1, 400 eV	0.09	2.70	0.04		
Ag, bond	−0.05	3.29	0.04	−0.43[f]	2.54[f]
Ag, hollow, 2 × 2 × 1, 400 eV	0.10	3.13	−0.02		
Ag, hollow	−0.05	3.44	0.06	−0.39[f]	2.61[f]

[a] The values have been calculated with spin polarization included. The **k**-point mesh used in our calculations is 3 × 3 × 1 and the cutoff energy is 500 eV unless otherwise stated. [b] A positive value is obtained when the perpendicularly most distorted C atom gets closer to the adsorbed cluster. See the text for details. [c] The corresponding PBE results are $E_{ads} = -0.14$ eV, $r_\perp = 2.73$ Å, and $\Delta Z_C = 0.11$ Å. [d] Data from ref 6. [e] The corresponding PBE results are $E_{ads} = -0.02$ eV, $r_\perp = 3.37$ Å, and $\Delta Z_C = 0.01$ Å. [f] Data from ref 7.

claimed that both metals favor atop and over bond sites on graphite surfaces.[6−8,10] Thus, the binding energies obtained for silver are −0.44, −0.43, and −0.39 eV for the atop, bond, and hollow sites, respectively. The corresponding values for gold are −0.67, −0.65, and −0.51 eV. A somewhat different conclusion was obtained in an earlier study according to which the bond site is the least stable for the silver atom, having a binding energy of −0.23 eV, whereas for the hollow and atop sites binding energies of −0.33 and −0.54 eV, respectively, are given.[9] All these results have been obtained with the LDA approximation. There is also a study on gold which gives a nonpolarized GGA adsorption energy of −0.15 eV for the atop site.[10] Adsorption energies of gold atoms on graphite are larger than those of silver, probably due to the larger electron affinity of gold.

Table 2 summarizes our results obtained using the potential PW91 for single atom cases. The values vary greatly depending on the level of calculation regarding the **k**-point mesh and cutoff energy selected. We have systematically checked the convergence of the calculation with respect to the **k**-point mesh and the plane wave cutoff. The 2 × 2 × 1 mesh and 400 eV cutoff, which converge well for the other systems studied in this work, are insufficient in the case of silver and gold atoms on the graphite surface. We found that a 3 × 3 × 1 mesh and a 500 eV cutoff were enough to produce well-converged results.

As stated earlier, previous DFT/LDA studies suggest that the silver atom adsorbs on the graphite atop site with an energy of about 0.44−0.54 eV in magnitude. Our GGA results are different. The adsorption of single silver atoms on graphite is not favored, because the adsorption energies obtained are close to zero. For gold, our computed energies and the value from ref 10 are somewhat larger in magnitude showing at least some degree of adsorption. This agrees with STM (scanning tunneling microscopy) results which indicate that gold atoms are less mobile than silver atoms.[30] Figure 1 shows the starting structures of the silver atom on a graphite surface (atop, bond, and hollow sites), and the corresponding results are given for the relaxed structures in Figure 2, where the silver atom has moved from the original positions.

As can be seen from Table 2, the adsorption energies obtained for gold and silver are almost constant regardless of whether the atom is adsorbed on an atop, a bond or a hollow site. Adsorption geometries are also given in Table 2. The parameter $r_\perp$ represents the perpendicular distance from the metal atom to the average *Z*-coordinate of the carbon atoms of the graphite surface (the *Z*-axis being perpendicular to the surface). The parameter ΔZ_C measures the deformation of the carbon sheet, and it is defined as the distance of the most distorted carbon atom from the average position of the carbon sheet. A positive value is obtained when the most distorted C atom gets closer to the adsorbed cluster, and a negative number occurs in the reverse situation. The $r_\perp$ distances using the PW91 exchange correlation functional are larger than those obtained with the LDA functionals in agreement with the behavior of the binding energies.

We have also repeated the calculations for the Ag and Au atoms adsorbed on the atop site employing the PBE and LDA (Ceperly−Alder parametrization) functionals. We have found that PBE gives results similar to those obtained with PW91 (see the footnotes c and e in Table 2 for our values of Ag and Au), and LDA gives results similar to those already found in previous studies (see Table 2 for our values of Ag).

4b. Dimers on Graphite. Six cases were considered for each metal dimer. The same adsorption sites were used as for single atoms (atop, bond, and hollow), and both the perpendicular and parallel orientations of the molecular axis were studied. The parallel orientations considered are shown in Figure 3.

For the silver dimer on graphite, all the calculations of which we are aware have been performed using the LDA approach.[7−9] The following binding energies have been reported in the literature: −0.51 eV (atop site), −0.52 eV (bond site), and −0.55 eV (hollow site).[8] They have been computed with eq 1 and only for the dimers oriented parallel to the graphite surface. Besides, the definitions of atop, bond, and hollow sites in ref 8 differ from ours (see Figure 3) such that our bond and hollow sites are their hollow (B) and bond (perpendicular) sites, respectively. Our atop site does not directly correspond to the sites in ref 8. In ref 7, all computed values are close to −3 eV, with the hollow position being slightly more favored than the other sites, and the average distance of the mass point center of the silver dimer from the graphite surface varying between 2.86 and 2.98 Å.[7] In this case, the values of the binding energy are obtained with eq 2, and the notation for the adsorption sites is the same as in ref 8. An earlier study, also using eq 2, gives values that are close to −2.3 eV, but with the hollow position being the least stable site.[9] The average distances varied in the range 2.90−2.97 Å. However, we are unable to provide a precise correspondence between the character of their and our sites due to notational problems in this reference.

Our calculations for the silver and gold dimers on a graphite surface were performed using the GGA approach. The results are in Table 3. The hollow site is the least stable position both for the parallel and perpendicular orientations of the silver dimer, but the differences are small (around 0.002 eV) in the case of the parallel dimer. The perpendicular orientation is preferred over the parallel one. The binding energies obtained with eq 1 are close to zero. The silver dimers are probably highly mobile along the graphite surface due to similar energies at different sites. Silver dimers on surfaces are seldom observed experimentally, which is consistent with high mobility. The average distance from the surface to the mass point center of the dimer

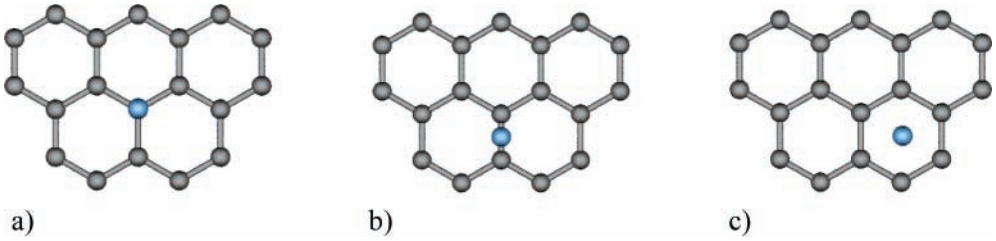

Figure 1. Starting structures for the silver atom on a graphite surface: (a) atop site (the metal atom is on the top of the central carbon atom); (b) bond site; (c) hollow site. There are 6 carbon atoms along the horizontal direction (*x*-axis) and 16 atoms along the vertical direction (*y*-axis) in a unit cell, and thus, there are altogether 96 carbon atoms per a unit cell.

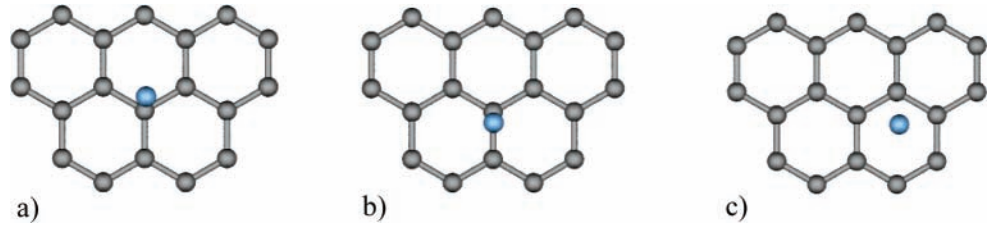

Figure 2. Relaxed structures for the silver atom on a graphite surface: (a) atop site; (b) bond site; (c) hollow site, calculated with a **k**-point mesh $3 \times 3 \times 1$ and a cutoff energy of 500 eV. For the unit cell size, see the caption of Figure 1.

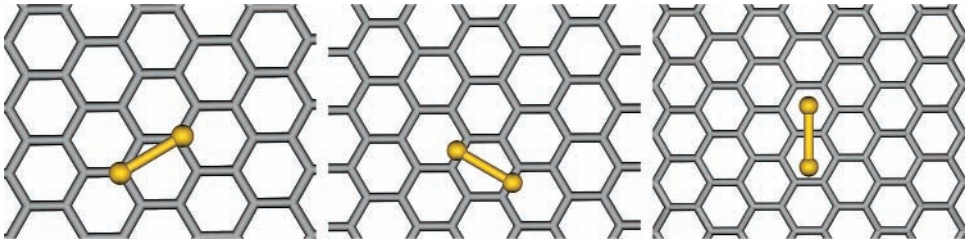

Figure 3. Parallel orientations of metal dimers studied in this work: left, parallel atop; middle, parallel bond; right, parallel hollow. The *y*-axis is located in the horizontal and the *x*-axis in the vertical direction.

TABLE 3: Adsorption Energies and Structures of the Studied Dimers[a]

dimer, site, orientation	E_1 (eV)	E_2 (eV)	r_{M-M} (Å)	$r_{COM-surf}$ (Å)[b]	ΔZ_C (Å)
Au_2, atop, ⊥	−0.55	−2.87	2.52	3.69	0.11
Au_2, atop, ⊥, 500 eV	−0.57	−2.89	2.52	3.68	0.10
Au_2, bond, ⊥	−0.55	−2.87	2.52	3.66	0.11
Au_2, hollow, ⊥	−0.25	−2.57	2.52	3.84	−0.01
Au_2, atop, ∥	−0.08	−2.40	2.53	3.43	−0.07
Au_2, bond, ∥	−0.08	−2.40	2.53	3.45	−0.07
Au_2, hollow, ∥	−0.08	−2.40	2.53	3.58	−0.07
Ag_2, atop, ⊥	−0.17	−1.97	2.57	3.88	0.03
Ag_2, atop, ⊥, 500 eV	−0.19	−1.99	2.57	3.86	0.03
Ag_2, bond, ⊥	−0.16	−1.96	2.57	3.86	0.01
Ag_2, hollow, ⊥	−0.10	−1.90	2.57	4.00	−0.03
Ag_2, atop, ∥	−0.06	−1.86	2.58	3.60	−0.08
Ag_2, bond, ∥	−0.06	−1.86	2.57	3.55	−0.07
Ag_2, hollow, ∥	−0.06	−1.85	2.57	3.54	−0.08

[a] All values in the table have been calculated with the potential PW91 using the **k**-point mesh $2 \times 2 \times 1$ and a cutoff 400 eV unless otherwise stated. [b] Difference between the dimer center of mass *Z*-coordinate and average surface *Z*-coordinate.

is also somewhat high, varying from 3.5−3.6 Å in the parallel orientation to 3.9−4.0 Å in the perpendicular one. The bond lengths in Ag_2 are almost identical to the gas-phase values. A slight deformation of the graphite occurs when Ag_2 is in the parallel orientation.

The **k**-point meshes $3 \times 3 \times 1$, $4 \times 4 \times 1$, and $5 \times 5 \times 1$ were also tested for the atop site of the perpendicular Ag_2 dimer. All these calculations gave the adsorption energies $E_2 = -1.97$ eV and $E_1 = -0.17$ eV, that is, practically the same values as those obtained with the **k**-point mesh $2 \times 2 \times 1$, so the $2 \times 2 \times 1$ mesh is large enough to obtain reliable results for dimers. The increase of the cutoff energy to 500 eV made only a small difference in the adsorption energies but a larger difference in the position of the dimer, particularly in the *y*-coordinates. This tendency is more pronounced in silver than in gold. The overall distances of the dimer center of mass *Z*-coordinate and average surface *Z*-coordinate remain almost constant.

The LDA has also been the method of choice for gold dimers on graphite in the literature. The values for the binding energy of the perpendicular dimer vary from −4 eV (atop and bond sites) to −3.8 eV (hollow site) using eq 2 (using eq 1, the values vary from −1.14 to −1.15 eV for the atop and bond sites to −0.92 eV for the hollow site), the average distance from the surface being 3.52−3.57 Å.[6,8] The values for the binding energy of the parallel dimer vary from −3.5 eV (bond site) to −3.6 eV (atop and hollow sites) using eq 2 (using eq 1, the values range from about −0.65 eV for bond site to −0.77 eV atop and hollow sites), the average distance being 2.63−2.85 Å.[6] Generally, it is concluded that the binding energies for the perpendicular case are larger than for the parallel orientation.

Our calculations (Table 3) indicate that the atop and bond sites of the perpendicular gold dimer are preferred over the hollow site. Additionally, the binding energies for all the parallel sites are smaller than for the perpendicular orientation. It has been suggested that the preference of gold dimers to locate perpendicularly is due to relativistic effects.[6] In the case of Au_2 parallel to the graphite surface, eq 1 gives values for the binding energies that are close to zero and even smaller in magnitude than those obtained for the gold monomer on graphite. This suggests that parallel Au_2 is unstable and most likely becomes perpendicular Au_2. The only case without deformation of the graphite is that in which Au_2 is in the perpendicular orientation

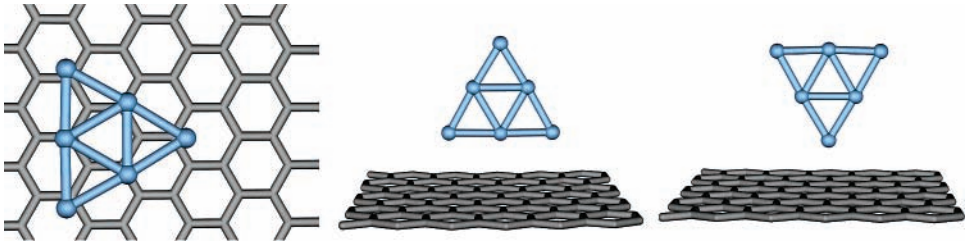

Figure 4. Orientation of planar M_6 clusters: left, parallel atop; middle, perpendicular edge-on; right, perpendicular vertex-on.

TABLE 4: Adsorption Energies and Structures of M_6 Clusters

cluster	E_1 (eV)	E_2 (eV)	E_3 (eV)	$r_{COM-surf}$ (Å)	r_{min} (Å)	ΔZ_C (Å)
Au_6 octa, atop	−0.56	−10.13	−0.72	4.34	2.34	0.23
Au_6 octa, bond	−0.55	−10.12	−0.72	4.33	2.42	0.21
Au_6 octa, hollow	−0.37	−9.94	−0.20	4.59	3.47	−0.04
Au_6 planar, atop, ∥	−0.16	−11.74	−0.11	3.88	3.88	−0.02
Au_6 planar, vertex atop, ⊥	−0.27	−11.86	−0.32	5.65	2.48	−0.10
Au_6 planar, edge atop, ⊥	−0.13	−11.71	−0.13	4.66	3.16	0.07
Ag_6 octa, atop	−0.86	−8.41	−0.35	4.02	2.52	0.14
Ag_6 octa, bond	−0.50	−8.05	−0.37	4.10	2.63	0.16
Ag_6 octa, hollow	−0.32	−7.87	−0.12	4.57	3.50	−0.03
Ag_6 planar, atop, ∥	−0.16	−8.92	−0.12	3.96	3.94	−0.03
Ag_6 planar, vertex atop, ⊥	−0.13	−8.89	−0.14	5.79	2.69	0.03
Ag_6 planar, edge atop, ⊥	−0.10	−8.87	−0.09	4.90	3.37	−0.10

cluster	width (Å)	height (Å)
Au_6 octa, atop	4.22	3.48
Au_6 octa, bond	4.19	3.54
Au_6 octa, hollow	4.57	2.90
Ag_6 octa, atop	4.81	2.67
Ag_6 octa, bond	4.76	2.75
Ag_6 octa, hollow	4.69	2.76

above the hollow site. The Au_2 bond lengths show an elongation of 0.011−0.026 Å compared to the gas-phase value. Experimentally, using the STM, gold dimers on graphite have been observed to span longer gold−gold distances than in the vacuum.[30] Overall, the gold dimer is somewhat closer to the surface than Ag_2. The average distance from the surface to the mass point center of the dimer varies from 3.4 to 3.8 Å.

4c. M_6 Adsorbed on Graphite. We have relaxed the octahedral M_6 clusters over the atop, bond, and hollow sites, and the planar M_6 structures for different orientations relative to the surface, as indicated in Figure 4. The results are summarized in Table 4. We make some general observations here before going into details. Both the planar and octahedral clusters avoid the hollow sites. The planar structures remain two-dimensional, and the octahedral clusters favor the atop site, where the lower side of the cluster is jagged. The distance between a planar cluster and the surface remains larger than in any of the three-dimensional cases if the planar cluster is placed parallel to the surface. Planar clusters are observed to be closest to the surface when the planar triangular cluster is placed perpendicular to the surface. According to the E_2 values, the octahedral structures are energetically less favored than the planar ones, which correlates well with the energy ordering of the clusters in the gas phase. On the other hand, the octahedral structures are more favorable than the planar ones as far as surface binding energy is concerned, i.e., according to the E_1 values.

The adsorption of planar clusters follows some general patterns. First, as mentioned above, the cluster geometries remain planar and they differ only slightly from the gas-phase structures. The largest changes in the nearest-neighbor bond lengths are 0.02 Å for Ag and 0.05 Å for Au. Second, the vertex-on orientation (see Figure 4) in Au_6 is energetically favored, whereas for Ag_6 there is no preferred orientation. All the planar adsorption geometries except the Au_6 vertex-on possess small binding energies, around 0.1−0.2 eV. The adsorption of planar Au_6 clusters on graphite has been studied with DFT/GGA methods recently.[11] Generally, our results for both the geometries and binding energies agree well with the published values, although the published parallel structure is bound slightly less strongly than in our work. Specifically, earlier works predict adsorption energies employing eq 1 and obtain −0.33 eV for the vertex-on, −0.15 eV for the edge-on, and −0.04 eV for the parallel orientation.

The largest deformations occur when octahedral clusters are above the atop or bond sites, where the octahedral symmetry is lost and the clusters become shorter in the direction perpendicular to the surface. Clusters above hollow sites are also flattened but retain the octahedral structure. The structural distortion is most pronounced in the Ag cluster, which is also adsorbed closest to the surface. The heights and widths of the M_6 octahedral structures adsorbed on graphite are given in Table 4. As a reference, the corresponding values in the vacuum are 3.96 and 3.95 Å for Ag_6 and Au_6 octahedrons, respectively. The distortions projected along the surface depend strongly on the adsorption site, as can be seen in Figure 5. There is a general tendency of the atoms to be adsorbed close to atop sites and away from hollow sites. The binding is also weaker when the clusters are adsorbed over the hollow site, and stronger over the atop site.

Graphite deformations are largest when octahedral clusters are placed on the atop and bond sites. The carbon atoms closest to the clusters are raised slightly from the plane of carbon atoms toward the cluster. For details, see Table 4.

The differences between adsorption sites are best described by the E_3 values, where the deformation of the surface and the cluster is included. The adsorption energy of the Au_6 octahedron is about 0.5 eV larger on the atop site than it is on the hollow site. The corresponding difference in silver is 0.2 eV.

We have also investigated charge changes in M_6 clusters. These were found to be small. A comparison of charge distributions of both adsorbed and free icosahedral clusters reveals that the metal atom directly above the surface carbon atom loses electron density to the surface. In Ag_6, the silver atom closest to a surface carbon atom shows a decrease of about 0.1 e in electron density compared to the same distorted adsorption structure in the vacuum without the surface. These changes are smaller in octahedral Au_6.

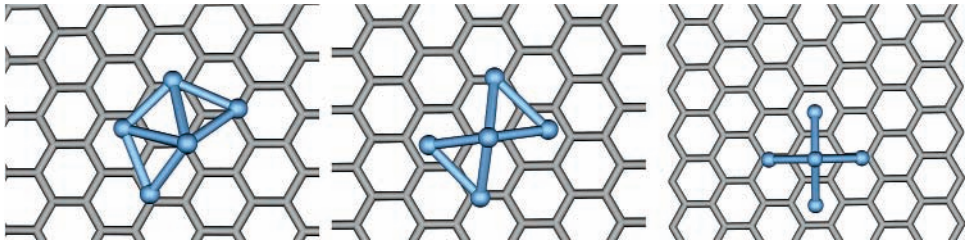

Figure 5. Optimized structures of Ag_6 octahedral clusters on graphite: left, adsorbed atop; middle, bond; right, hollow. The sixth atom is lying below the atom in the center of the cluster.

TABLE 5: Adsorption of the Icosahedral M_{13} Clusters

cluster	E_1 (eV)	E_2 (eV)	E_3 (eV)	$r_{COM-surf}$ (Å)	$r_{closest}$ (Å)	ΔZ_C (Å)
Au_{13} ico	−2.76	−27.72	−0.21	5.56	3.33	0.07
Ag_{13} ico	−1.10	−21.80	−0.31	5.64	2.51	0.07

4d. M_{13} Clusters Adsorbed on Graphite. We have considered only the icosahedrons of the M_{13} structures due to computational limitations. Large surface slabs would have been required to prevent clusters in adjacent cells from interacting in planar structures. The closest distance between metal atoms on adjacent clusters is 9.56 Å (Au) and 9.25 Å (Ag). The contribution from a neighboring cell is small, the bond energy of Au_2 at 9 Å is less than 4 meV. The results for the icosahedrons are given in Table 5.

There are large distortions when compared with the gas-phase structures (see Figure 6). The largest changes occur in silver. Unrealistic adsorption energies are obtained if vacuum structures are used. The best way to deal with adsorption is to use the distorted structures, i.e., E_3, where the structural distortion caused by adsorption and the interaction between the surface and the cluster can be separated. For example, E_1 of gold is almost −3 eV. This indicates that there is strong chemical bonding to the surface, which is unrealistic. The large absolute value of E_1 is due to the large structural changes of the cluster upon adsorption. The same occurs in the octahedral clusters, where E_1 is as small as −0.86 eV in Ag_6. The computed E_1 is smaller than E_3 because the total energy of the adsorbed structure in the gas phase is smaller than the icosahedral energy in the gas phase. It should be noted that the details of the optimized cluster structure on graphite might depend on the initial starting structure and orientation, but further investigations are left for future work.

4e. Van der Waals Energy Contributions.

C_6 Coefficients. We have used the atomic polarizabilities from refs 31−33 and the van der Waals radii from ref 34 to evaluate the C_6 and R_0 coefficients. For the C atom, we have employed the Cbr polarizability by Miller,[31] which has been obtained empirically from molecules with the C atoms in their sp^2 hybridization state. This result should suit our problem better than a value obtained from a series of molecules in which C can be in any of its hybridization states. Some other authors[23] have adopted the same view, and good results have been obtained when compared with Møller−Plesset second-order perturbation theory calculations.

The C_6 coefficients and van der Waals radii used in Grimme's approach were taken from ref 18. The coefficients are presented in Table 6. Altogether four different sets of coefficients for the Ag clusters and one set for the Au clusters on graphite are presented in the same table.

There is a large scatter, of almost 1 order of magnitude, in the C_6 coefficients of Ag in Table 6. Set 2, in particular, differs

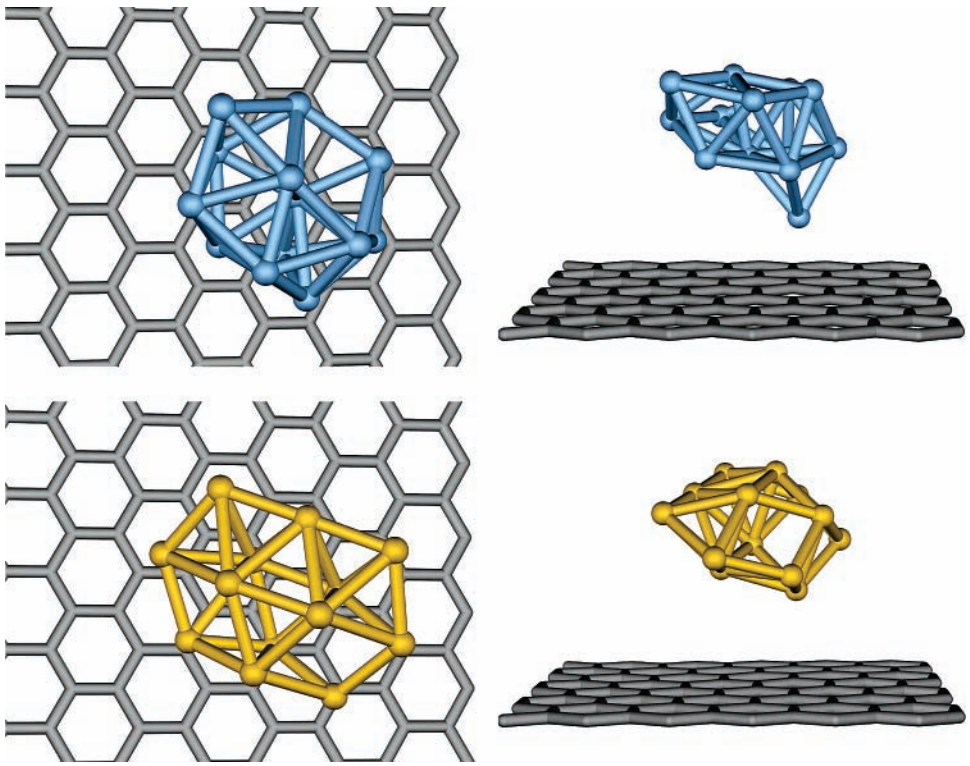

Figure 6. Optimized structures of M_{13} icosahedral clusters: top, Ag_{13} cluster; bottom, Au_{13} cluster.

TABLE 6: Sets of Coefficients C_6 and R_0 Used To Estimate Van Der Waals Energies[a]

Ag_n on Graphite

	set 1			set 2			set 3			set 4		
$\alpha\beta$	CC	AgAg	CAg	CC	AgAg	CAg	CC	AgAg	CAg	CC	AgAg	CAg
$C_6^{(\alpha\beta)}$ (eVÅ^6)	32.37	486.14	125.24	32.37	60.60	26.60	32.37	389.22	110.68	20.24	285.25	75.97
$R_0^{(\alpha\beta)}$ (Å)	3.40	3.44	3.42	3.40	3.44	3.42	3.40	3.44	3.42	2.90	3.28	3.09

Au_n on Graphite

	set 1		
$\alpha\beta$	CC	AuAu	CAu
$C_6^{(\alpha\beta)}$ (eVÅ^6)	32.37	277.05	94.63
$R_0^{(\alpha\beta)}$ (Å)	3.40	3.32	3.36

[a] Set 1: Elstner's procedure with C_6(Ag) and C_6(Au) estimated via eq 5. Set 2: Elstner's procedure with C_6(Ag) taken from ref 26. Set 3: Elstner's procedure with C_6(Ag) taken from ref 27. Set 4: Grimme's method.

from the others. In this case, the C_6 coefficient of Ag is taken from ref 26, where the result is obtained for a system with one silver atom interacting with an Ag(100) surface. The method employed is based on expressions derived by Persson and Zaremba.[35] These authors noticed that the calculated coefficients are smaller than those employed in the previous molecular dynamics simulations of the same system. However, they observed that a good representation of the growing process of metal at large angles of incidence is obtained with their coefficients. Although the other three sets of coefficients for the Ag clusters on graphite have more in common with each other, there are still differences. In set 3, the C_6 coefficient of Ag is from ref 27, where Ag_2Te was studied with high-level *ab initio* calculations, and the C_6 coefficient for Ag is evaluated by representing the Ag−Ag potential as a polynomial expansion. The result is 20% smaller in magnitude than our estimation using eq 5. Finally, set 4, whose coefficients have been taken from Grimme's work, differ somewhat from set 1, but it is not easy to predict what effect it will have on the van der Waals energies due to the different damping functions employed.

Binding Energies. We have taken the coefficients from the previous section and the geometries computed with the DFT when evaluating van der Waals energies. The summation in eq 4 has been carried out considering only the atoms in the unit cell. The binding energies originating from van der Waals dispersion have been calculated following the definitions given in eqs 1 and 3, which emphasize different energetical aspects, particularly when comparing the same cluster absorbed at different sites. The definition given in eq 1, which includes the cluster's relaxation energy, gives the most energetically favorable site and eq 3 gives the most physically meaningful van der Waals contribution to the adsorption energy. The definition given in eq 2 is not suitable for the present purposes, because the semiclassical models only include two-body terms. We have included silver−silver, carbon−carbon, and silver−carbon interactions. The results obtained with eqs 1 and 3 are similar, the differences being generally some hundredths of an electronvolt, which indicates that van der Waals energies vary slowly with the displacement of the atoms in our system. In Table 7, we give mainly the binding energies obtained with eq 1, because we wish to emphasize the relative stability of a cluster adsorbed on different sites. However, for the adsorption of the three-dimensional M_6 and M_{13} clusters, the results obtained with eq 1 and eq 3 differ somewhat; see the footnote in Table 7 for numerical details. This is related to the large structural changes of three-dimensional clusters upon adsorption.

From the results in Table 7, it can be seen that the total binding energy depends greatly on the set of parameters used and is especially sensitive to the values of the C_6 coefficients, which are responsible for the strength of van der Waals

TABLE 7: Van der Waals Binding Energies for Ag and Au Clusters on Graphite[a]

Ag_n on Graphite

cluster, site, orientation	set 1 E_1 (eV)	set 3 E_1 (eV)	set 4 E_1 (eV)	set 2 E_1 (eV)	DFT/PW91 E_1 (eV)
Ag, atop	−0.77	−0.68	−0.56	−0.18	−0.05
Ag, bond	−0.78	−0.69	−0.55	−0.18	−0.05
Ag, hollow	−0.69	−0.61	−0.42	−0.16	−0.05
Ag_2, atop, ⊥	−0.88	−0.78	−0.64	−0.20	−0.17
Ag_2, bond, ⊥	−0.90	−0.79	−0.65	−0.20	−0.16
Ag_2, hollow, ⊥	−0.83	−0.74	−0.60	−0.19	−0.10
Ag_2, atop, ∥	−0.83	−0.73	−0.51	−0.19	−0.06
Ag_2, bond, ∥	−0.87	−0.77	−0.53	−0.20	−0.06
Ag_2, hollow, ∥	−0.88	−0.78	−0.54	−0.20	−0.06
Ag_6 octahedral, atop	−1.86[b]	−1.66	−1.20	−0.42	−0.86
Ag_6 octahedral, bond	−1.85[b]	−1.64	−1.15	−0.41	−0.50
Ag_6 octahedral, hollow	−1.63[b]	−1.42	−0.76	−0.33	−0.32
Ag_6 planar, atop, ∥	−1.75	−1.55	−1.07	−0.39	−0.16
Ag_6 planar, atop, vertex	−1.05	−0.93	−0.73	−0.24	−0.13
Ag_6 planar, atop, edge	−1.76	−1.55	−1.05	−0.39	−0.10
Ag_{13} icosahedral, atop	−1.43[b]	−1.29	−0.71	−0.35	−1.10

Au_n on Graphite

cluster, site, orientation	set 1 E_1 (eV)	DFT/PW91 E_1 (eV)
Au, atop	−0.61	−0.22
Au, bond	−0.51	−0.22
Au, hollow	−0.40	−0.22
Au_2, atop, ⊥	−0.74	−0.55
Au_2, bond, ⊥	−0.74	−0.55
Au_2, hollow, ⊥	−0.66	−0.25
Au_2, atop, ∥	−0.76	−0.08
Au_2, bond, ∥	−0.74	−0.08
Au_2, hollow, ∥	−0.66	−0.08
Au_6 octahedral, atop	−1.42[b]	−0.56
Au_6 octahedral, bond	−1.42[b]	−0.55
Au_6 octahedral, hollow	−1.21[b]	−0.37
Au_6 planar, atop, ∥	−1.44	−0.16
Au_6 planar, atop, vertex	−0.88	−0.27
Au_6 planar, atop, edge	−1.63	−0.13
Au_{13} icosahedral, atop	−0.39[b]	−2.76

[a] Set 1: Elstner's procedure with C_6(Ag) and C_6(Au) estimated via eq 5. Set 2: Elstner's procedure with C_6(Ag) taken from ref 26. Set 3: Elstner's procedure with C_6(Ag) taken from ref 27. Set 4: Grimme's method. All values are in eV. [b] Values obtained with eq 3 are Ag_6 octahedral atop (−1.98), bond (−1.89), and hollow (−1.32). For Au_6 octahedral atop (−1.26), bond (−1.29), and hollow (−1.02). For Ag_{13} icosahedral atop (−1.75). For Au_{13} icosahedral atop (−1.33). Set 1 was used for Ag.

interactions. There is a large uncertainty in the value of the C_6 coefficient for Ag, and more research is needed to compute a reliable value. For Au the situation is not better, because the only coefficients available seem to be those estimated in this work. Therefore, in giving a physical interpretation for the results, we deal with relative energies.

It is also clear from the results in Table 7 that the van der Waals contribution to the binding energy dominates over the DFT contribution in many cases. However, this should be taken with caution because, first, the model we use to estimate the van der Waals energies is crude, and second, there is a large uncertainty in the values of the C_6 coefficient of the metallic atoms. Despite these reservations, we believe that van der Waals contributions must be included when studying metal clusters on the graphite surface.

The inclusion of van der Waals dispersion energies on top of DFT energies increases the stability for the atomic adsorptions. The three adsorption sites, atop, bond, and hollow possess similar DFT binding energies. This is also the case in the van der Waals contributions, although the hollow site might be slightly less favored than atop and bond sites.

For the dimer adsorptions, the DFT results indicate a preference for the perpendicular orientation of the dimer on the surface. The van der Waals energies hardly change from the parallel to perpendicular orientation, so the conclusion obtained with DFT remains valid.

For the octahedral clusters with 6 atoms, dispersion contributions to the binding energies are the smallest for the hollow site. The same trend is observed in the case of DFT binding energies. For the planar structures, the DFT favor the Au_6 vertex adsorption, predicting it to be approximately 0.1 eV more stable than the others. In this case, dispersion predicts the contrary behavior: the Au_6 vertex is more than 0.5 eV higher in energy than the other two planar adsorption geometries. Even considering the uncertainty in the dispersion results from our estimated C_6 coefficient of gold, it is likely that the dispersion contribution to the binding energy determines the relative energetics. For the Ag_6 planar adsorptions, the DFT predicts a similar binding energy for the three sites studied, and the estimate of the dispersion forces suggests again that vertex adsorption is unfavored, its binding energy being $0.7-0.15$ eV larger than in the other adsorption geometries. This might be the dominant effect on the total binding energy. Finally, for the adsorption of the clusters with 13 atoms, the dispersion again contributes to the stability of the system.

5. Conclusions

We have used the density functional theory to evaluate the energetics of the adsorption of silver and gold clusters on a single carbon sheet of graphite. These calculations exclude the effects of dispersion forces, which have been investigated with an empirical model. We can summarize some of the conclusions from the electronic structure calculations as follows. There are significant structural changes in the larger metal clusters, especially with silver, on the graphite sheet when compared with isolated clusters. Therefore, unlike in many molecular systems, the usual definition of the adsorption energy is not necessarily the best, and the most physically appealing definition is often the total energy of the system (cluster and surface together at the minimum energy configuration) minus both the isolated cluster energy at the adsorbed configuration and the graphite sheet energy at the adsorbed configuration.

A detailed inspection of the electronic structure calculation results reveal that (1) the hollow sites are less favorable than the atop or bond sites, (2) adsorption energies of planar structures are smaller than in octahedral cases and thus the adsorption of three-dimensional structures is preferred to that of planar structures, (3) planar structures favor the vertex-on approach to the surface, (4) small deformations of the graphite sheet toward the cluster often occur when the cluster is adsorbed on the atop/bond sites and the deformations are often in the opposite direction when the adsorption occurs on the hollow site, and (5) due to the relatively weak interactions with the surface, the clusters have a tendency to aggregate, which has also been observed experimentally.

There are two conclusions concerning the current state-of-the-art semiempirical approaches to include dispersion on top of the DFT. First, accurate C_6 coefficients are not available for silver or gold, so more research is needed in this area. Second, the semiempirical dispersion energies obtained with different C_6 coefficients behave similarly, but there are differences in the total strength of the interaction. It is also interesting to compare the energies from the density functional theory and the empirical treatment of dispersion forces. Probably, the most striking difference occurs in the case of perpendicular adsorption of the planar triangular Ag_6 and Au_6. The DFT results indicate that on the atop site the triangle is adsorbed with the vertex toward the surface. On the contrary, the dispersion forces favor the structure where the edge is pointing toward the surface. We conclude that for systems such as those studied here, it might be a bad approximation to neglect dispersion energies. Our results indicate that dispersion forces could have an important effect on the stabilization of metal clusters adsorbed on the graphite surface.

Acknowledgment. We are grateful to Dr. Joseph Guss for comments on our manuscript. We thank the Academy of Finland, the Finnish Ministry of Education, and the CMS Center of Excellence for financial support. We also thank the CSC Scientific Computing Ltd for providing computing time.

References and Notes

(1) Morse, M. D. *Chem. Rev.* **1986**, *86*, 1049.
(2) Häkkinen, H.; Yoon, B.; Landman, U.; Li, X.; Zhai, H. J.; Wang, L. S. *J. Phys. Chem. A* **2003**, *107*, 6168.
(3) Wang, J.; Wang, G.; Zhao, J. *Phys. Rev. B* **2002**, *66*, 035418.
(4) Fournier, R. *J. Chem. Phys.* **2001**, *115*, 2165.
(5) Oviedo, J.; Palmer, R. E. *J. Chem. Phys.* **2002**, *117*, 9548.
(6) Wang, G. M.; BelBruno, J. J.; Kenny, S. D.; Smith, R. *Phys. Rev. B* **2004**, *69*, 195412.
(7) Wang, G. M.; BelBruno, J. J.; Kenny, S. D.; Smith, R. *Surf. Sci.* **2003**, *541*, 91.
(8) Smith, R.; Nock. C.; Kenny, S. D.; Belbruno, J. J.; Di Vece, M.; Palomba, S.; Palmer, R. E. *Phys. Rev. B* **2006**, *73*, 125429.
(9) Duffy, D. M.; Blackman, J. A. *Surf. Sci.* **1998**, *415*, L1016.
(10) Jensen, P.; Blase, X.; Ordejón, P. *Surf. Sci.* **2004**, *564*, 173.
(11) Akola, J.; Häkkinen, H. *Phys. Rev. B* **2006**, *74*, 165404.
(12) Rydberg, H.; Lundqvist, B. I.; Langreth, D. C.; Dion, M. *Phys. Rev. B* **2000**, *62*, 6997.
(13) Rydberg, H.; Dion, M.; Jacobson, N.; Schröder, E.; Hyldgaard, P.; Simak, S. I.; Langreth, D. C.; Lundqvist, B. E. *Phys. Rev. Lett.* **2003**, *91*, 126402.
(14) Andersson, Y.; Langreth, D. C.; Lunqvist, B. I. *Phys. Rev. Lett.* **1996**, *76*, 102.
(15) Hasegawa, M.; Nishidate, K. *Phys. Rev. B* **2004**, *70*, 205431.
(16) Pisani, C.; Busso, M.; Capecchi, G.; Casassa, S.; Dovesi, R.; Maschio, L.; Zicovich-Wilson, C.; Schütz, M. *J. Chem. Phys.* **2005**, *122*, 094113.
(17) Elstner, M.; Hobza, P.; Frauenheim, T.; Suhai, S.; Kaxiras, E. *J. Chem. Phys.* **2001**, *114*, 5149.
(18) Grimme, S. *J. Comp. Chem.* **2006**, *27*, 1787.
(19) Blöchl, P. E. *Phys. Rev. B* **1994**, *50*, 17953.
(20) Kresse, G.; Joubert, J. *Phys. Rev. B* **1999**, *59*, 1758.

(21) Perdew, J. P.; Chevary, J. A.; Vosko, S. H.; Jackson, K. A.; Pederson, M. R.; Singh, D. J.; Fiolhais, C. *Phys. Rev. B* **1992**, *46*, 6671.
(22) Liu, Z. F.; Yim, W. L.; Tse, J. S.; Hafner, J. *Eur. Phys. J. D* **2000**, *10*, 105.
(23) Williams, R. W.; Malhotra, D. *Chem. Phys.* **2006**, *327*, 54.
(24) Halgren, T. A. *J. Am. Chem. Soc.* **1992**, *114*, 7827.
(25) Slater, J. C.; Kirkwood, J. G. *Phys. Rev.* **1931**, *37*, 682.
(26) Amar, J. G. *Phys. Rev. B* **2003**, *67*, 165425.
(27) Surong, Q.-M.; Zhao, Y.; Jing, X.; Li, X.; Su, W. *Int. J. Quantum Chem.* **2004**, *100*, 293.
(28) Hasegawa, M.; Nishidate, D. *Phys. Rev. B* **2004**, *70*, 205431.
(29) Huber, K. P.; Herzberg, G. *Molecular Spectra and Molecular Structure 4. : Constants of Diatomic Molecules*; Van Nostrand Reinhold: New York, 1979.
(30) Ganz, E.; Sattler, K.; Clarke, J. *Surf. Sci.* **1989**, *219*, 33.
(31) Miller, K. J. *J. Am. Chem. Soc.* **1990**, *112*, 8533.
(32) Neogrády, P.; Kellö, V.; Urban, M.; Sadlej, A. J. *Int. J. Quantum Chem.* **1996**, *63*, 557.
(33) Henderson, M.; Curtis, L. J.; Matulioniene, R.; Ellis, D. G.; Theodosiou, C. E. *Phys. Rev. A* **1997**, *56*, 1872.
(34) http: //web.mit.edu/hg_v1.2.1/distrib/mercury_1_2_1/docs/mercury/PortableHTML/mercurydocn144.html.
(35) Persson, B. N. J.; Zaremba, E. *Phys. Rev. B* **1984**, *30*, 5669.